ISSN 0023-1584, Kinetics and Catalysis, 2019, Vol. 60, No. 6, pp. 842–850. © Pleiades Publishing, Ltd., 2019.
Russian Text © The Author(s), 2019, published in Kinetika i Kataliz, 2019, Vol. 60, No. 6, pp. 816–824.

$PdIn/Al_2O_3$ Intermetallic Catalyst: Structure and Catalytic Characteristics in Selective Hydrogenation of Acetylene

P. V. Markov[a, b], A. V. Bukhtiyarov[b, c], I. S. Mashkovsky[a], N. S. Smirnova[b], I. P. Prosvirin[b], Z. S. Vinokurov[b, c], M. A. Panafidin[b], G. N. Baeva[a], Ya. V. Zubavichus[b, c], V. I. Bukhtiyarov[b], and A. Yu. Stakheev[a, *]

[a] *Zelinsky Institute of Organic Chemistry, Russian Academy of Sciences, Moscow, 119991 Russia*
[b] *Boreskov Institute of Catalysis, Siberian Branch, Russian Academy of Sciences, Novosibirsk, 630090 Russia*
[c] *Novosibirsk State University, Novosibirsk, 630090 Russia*
**e-mail: st@ioc.ac.ru*

Received April 29, 2019; revised May 10, 2019; accepted May 13, 2019

Abstract—The structure and catalytic characteristics of a bimetallic catalyst containing Pd_1In_1 nanoparticles deposited on the surface of γ-Al_2O_3 were studied. The formation of intermetallic nanoparticles was determined by X-ray diffraction analysis and confirmed by X-ray photoelectron spectroscopy and IR spectroscopy of adsorbed CO. In the hydrogenation of acetylene in excess ethylene, $PdIn/Al_2O_3$ had significantly higher selectivity of ethylene formation (~86%) than monometallic Pd/Al_2O_3 (~35%). The high selectivity of $PdIn/Al_2O_3$ is explained by two factors: (1) the formation of monatomic Pd_1 sites isolated from one another by In atoms and (2) the change in the electronic state of Pd atoms in the intermetallic nanoparticles.

Keywords: gas-phase hydrogenation of acetylene, bimetallic catalysts, nanoparticles, catalyst structure, palladium, indium, isolated Pd sites, intermetallics

DOI: 10.1134/S0023158419060065

INTRODUCTION

Rapid progress in modern chemistry gives rise to new promising trends in the development and creation of catalytic materials with specific and sometimes unique properties. Intermetallic compounds have great potential in this regard. Their characteristics were discussed in detail in recent reviews [1–4]. The main distinction of intermetallic compounds is their specific metallic properties [5]. Due to the high degree of ordering and crystal structure stability, a unique ensemble of active sites with identical homogeneous structures form on the catalyst surface, so that the reaction parameters can be controlled already during the catalyst synthesis [1, 4].

The PdGa intermetallics is one of the most thoroughly studied catalytic systems which has a set of unique catalytic properties. The structure of PdGa catalysts and its effect on the catalytic characteristics were studied by Schlögl [6–13], Tsyrul'nikov [14–19], and Furukawa [20] and reviewed in [21]. It was noted that PdGa intermetallics have extremely high selectivity in hydrogenation of acetylenes and are promising catalysts for large-scale catalytic removal of C_2H_2 impurities and homologs from the pyrolysis ethane-ethylene fractions. All researchers agree that the high selectivity of PdGa systems results from the formation of monatomic Pd_1 sites on the catalyst surface, isolated from one another by inactive Ga atoms [7–9, 17, 20].

A significant disadvantage of the PdGa compositions is low stability of the Ga component against oxidation. Even short-term contact of the preliminarily reduced PdGa catalyst with air (e.g., during the catalyst unloading or loading in the reactor), Ga is oxidized, forming oxide followed by destroying of bimetallic particles. As a result, the yield of the desired reaction product and hence the selectivity of catalytic hydrogenation decrease [12].

Indium [22] is regarded as a possible alternative to Ga for the synthesis of intermetallic palladium catalysts. It is an electronic analog of gallium and also belongs to Group XIII of the periodic table. It forms a series of intermetallic compounds with Pd, which have

Abbreviations: Pd_1 sites—palladium atoms isolated from one another by the atoms of the second metal (In); XRD—X-ray diffraction analysis; S_{sp}—specific surface area; IR-CO—IR spectroscopy of adsorbed CO; a. b.—absorption band; XPS—X-ray photoelectron spectroscopy; $X_{C_2H_2}$—conversion of acetylene; $S_{C_2H_4}$—selectivity of ethylene formation; $T_{100\%}$—temperature at which 100% conversion of C_2H_2 is achieved; $S_{90\%}$—selectivity of ethylene formation at 90% conversion of C_2H_2; BE—binding energy; E_a—activation energy.

various compositions and structures [23, 24]. We showed that active Pd_1 sites, isolated from one another by indium atoms, can form on the surface of Pd_1In_1 intermetallic nanoparticles [25–27]. The advantage of PdIn-based catalysts is their increased stability to oxidation compared to that of PdGa systems, which is due to the lower oxophilicity of indium. The oxidative potential is ~–0.3 V for In and ~–0.5 V for gallium [1, 28]. Our previous studies showed that PdIn catalysts with a structure of isolated Pd_1 sites have high selectivity in liquid-phase hydrogenation of substituted alkyne compounds [29] and retain it even after storage of the catalysts in air without any special precautions (storage under argon, use of boxes with an inert atmosphere, etc.) [30].

The goal of this study was to investigate the properties of the bimetallic PdIn catalyst in the industrially important reaction of gas-phase hydrogenation of acetylene in excess ethylene and to compare the catalytic characteristics with the results of characterization of the catalyst structure by XRD, IR–CO, and XPS. The catalyst was prepared from the heterometallic acetate complex $Pd(\mu\text{-}AcO)_4In(AcO)$ used as a precursor. Earlier, we found that this methodology afforded catalytic systems with highly ordered active sites [26, 27, 29].

EXPERIMENTAL

Preparation of Catalysts

The PdIn/Al_2O_3 bimetallic catalyst was obtained by impregnation of previously calcined γ-Al_2O_3, (Sasol, S_{sp} = 56 m^2/g, T_{calc} = 600°C, 3 h) from an acetic acid solution of the $Pd(\mu\text{-}AcO)_4In(AcO)$ complex (pH 2.8). The support was impregnated seven times because of its moisture capacity and solubility in acetic acid. After impregnation, the catalyst was dried in air at room temperature and then reduced in a flow of 5 vol % H_2 + Ar (550°C, 3 h). The metal content in the final catalyst was 2.5 wt % Pd and 2.7 wt % In. The use of the high concentration of the active component was dictated by the necessity of physicochemical analysis.

The monometallic Pd/Al_2O_3 and In/Al_2O_3 reference catalysts were prepared by impregnating γ-Al_2O_3 with aqueous $Pd(NO_3)_2$ and $In(NO_3)_3$ solutions. After drying at room temperature, the samples were calcined in an air flow (500°C, 4 h) and reduced in a flow of 5 vol % H_2 + Ar (700°C, 1 h).

X-Ray Diffraction Analysis

After the reduction of the Pd/Al_2O_3 and PdIn/Al_2O_3 catalyst samples in a 10% H_2/He flow at 500°C for 1 h, the X-ray diffraction patterns were recorded on a D8 Advance laboratory diffractometer (Bruker, Germany) using Cu$K\alpha$ radiation (λ = 1.5418 Å, Ni$K\beta$ filter), a Lynxeye linear detector (Bruker, Germany), and an XRK-900 high-temperature in situ cell (Anton Paar, Austria). The measurements were performed at room temperature after cooling the sample in the same medium. The scan range in the θ/θ configuration was 35°–90° at a step of 0.03° and accumulation time per point of 5 s. The crystallite sizes were evaluated using the Selyakov–Scherrer formula [31] with allowance for the instrumental broadening of the diffractometer.

IR Spectroscopy of Adsorbed CO

The IR diffuse reflectance spectra of adsorbed CO were recorded using a Tensor 27 FTIR spectrometer (Bruker, Germany) equipped with an in situ Harrick Diffuse Reflectance Kit (Harrick Scientific, United States) and an MCT detector (Bruker, Germany). The powdered catalyst was placed in a thermostated cell with CaF_2 glasses and heated to 500°C in an argon flow (30 mL/min), then reduced at 500°C for 1 h in a flow of 5% H_2/Ar (30 mL/min) and cooled to 200°C in the same mixture. Further cooling to 50°C was performed in an argon flow, after which the background spectrum was recorded. The spectra of adsorbed CO were recorded at 50°C in a flow of 0.5 vol % CO/He (500 scans, resolution 4 cm^{-1}).

X-Ray Photoelectron Spectroscopy

The XPS spectra were measured on a SPECS photoelectron spectrometer using non-monochromated Al$K\alpha$ radiation ($h\nu$ = 1486.6 eV, 150 W). The binding energy scale (BE) was pre-calibrated using the positions of the photoelectron of Au4$f_{7/2}$ (BE = 84.0 eV) and Cu2$p_{3/2}$ (BE = 932.67 eV) core level peaks. The charging effect arising during electron photoemission was taken into account by the internal standard method using the Al2p line (BE = 74.5 eV) of the support (Al_2O_3) [32]. All the spectra were measured at an analyzer pass energy of 20 eV. The samples were preliminarily reduced in hydrogen ($P(H_2)$ = 100 mbar, T = 500°C, t = 1 h) in the high pressure cell of the photoelectron spectrometer, which allows the pretreatment of samples in various gaseous media at pressures of up to 1 atm and temperatures of 50–500°C. For pretreatment, the samples were rubbed into a stainless steel gauze spot-welded to a standard sample holder. After cooling in hydrogen and evacuation, the samples were transferred to the analyzer chamber, where measurements were made.

The relative contents of elements on the catalyst surface and the ratio of their atomic concentrations were determined from the integrated intensities of the

photoelectron lines corrected by their respective atomic sensitivity factors [33].

Gas-Phase Hydrogenation of Acetylene

Acetylene was hydrogenated into ethylene in a flow-type quartz reactor (inner diameter 4 mm) at atmospheric pressure using a gas mixture of 0.5 vol % C_2H_2, 46.4 vol % C_2H_4, 2.6 vol % H_2, and 50.5 vol % Ar (the total flow rate was 64 mL/min). The temperature was increased stepwise in the range 25–150°C and monitored with a chromel–alumel thermocouple placed in the catalyst bed. The reaction products were analyzed on a Crystallux-4000M chromatograph (Meta-Chrom, Russia) equipped with a CP7518 capillary column (CP-Al_2O_3/KCl, 50 m × 0.53 mm, 10 μm) and a flame ionization detector.

The conversion of acetylene $X_{C_2H_2}$ was calculated as the ratio of the amount of changed acetylene to the amount of acetylene at the reactor inlet by the equation

$$X_{C_2H_2} = \frac{(C_2H_{2in} - C_2H_{2out})}{C_2H_{2in}},$$

where C_2H_{2in} and C_2H_{2out} are the peak areas of acetylene before and after the reaction, respectively.

The selectivity of ethylene formation was determined by the equation

$$S_{C_2H_4} = \frac{(C_2H_{2in} - C_2H_{2out})}{((C_2H_{2in} - C_2H_{2out}) + C_2H_6)},$$

where C_2H_6 is the concentration of ethane.

Before loading to the reactor, each catalyst was pelletized and fractionated (fraction size 0.2–0.4 mm). After loading, the samples were reduced in a 5% H_2/Ar flow at 550°C for 1 h followed by cooling down to room temperature in an N_2 flow (purity 5.0).

RESULTS AND DISCUSSION

X-Ray Diffraction Analysis

The XRD patterns of the catalysts are shown in Fig. 1. After reduction in hydrogen, the signals of the following phases were observed in addition to the reflections of the support: Pd_1In_1 intermetallic phase (cubic structure of the CsCl type, space group *Pm*-3*m*, $a = 3.23(4)$ Å (3.246 Å for PdIn 59473-ICSD)) for the PdIn/γ-Al_2O_3 sample; palladium hydride PdH_x phase (space group *Fm*-3*m*, $a = 4.02(7)$ Å (4.03 Å for palladium hydride $PdH_{0.64}$ 201089-ICSD and 3.876 Å for metallic palladium Pd 64922 ICSD) for the Pd/γ-Al_2O_3 sample. The presence of the palladium hydride phase is explained by the high ability of palladium to accumulate hydrogen and the cooling of the samples in a hydrogen-containing atmosphere. The hydrogen effect on the PdIn intermetallic phase was not revealed. Evaluation of the crystallite size by the Selyakov–Scherrer formula using PdIn(100) and Pd(111) reflections gave 2–3 nm for both phases.

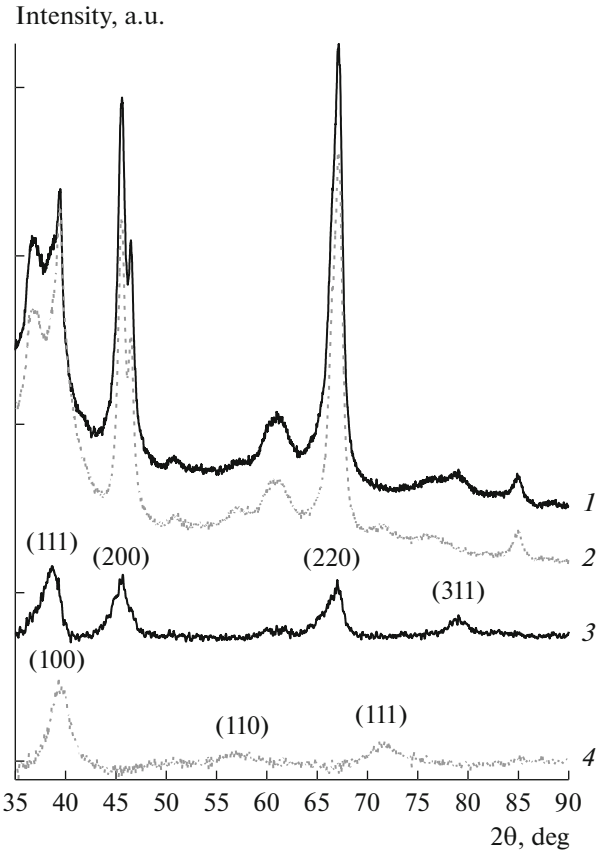

Fig. 1. Diffraction patterns for the (*1*) Pd/Al_2O_3 and (*2*) PdIn/Al_2O_3 samples after reduction in a hydrogen flow at 500°C. For clarity, the difference curves (*3* and *4*, respectively) are shown for these samples after subtracting the curve of the support. The Miller indices (*hkl*) are shown for the dominant PdH_x and PdIn phases.

FTIR Spectroscopy of Adsorbed CO

The FTIR spectra of adsorbed CO for the monometallic palladium catalyst show two broad asymmetric absorption bands (a. b.) in the range 2200–1800 cm^{-1}, one of which (2100–2050 cm^{-1}) corresponds to the CO molecules linearly adsorbed on palladium atoms, and the other (2000–1900 cm^{-1}) indicates the presence of bridging CO forms adsorbed on different faces of the metal particles (spectrum *1*, Fig. 2) [34]. The band in the region of ~1900–1800 cm^{-1} presumably corresponds to the tricoordinate forms of CO on the Pd surface. The maximum of a.b. for the linear form of CO at 2088 cm^{-1} is typical for monometallic palladium catalysts [35]. The high intensity of the peak related to the multi-coordinate forms of adsorbed CO

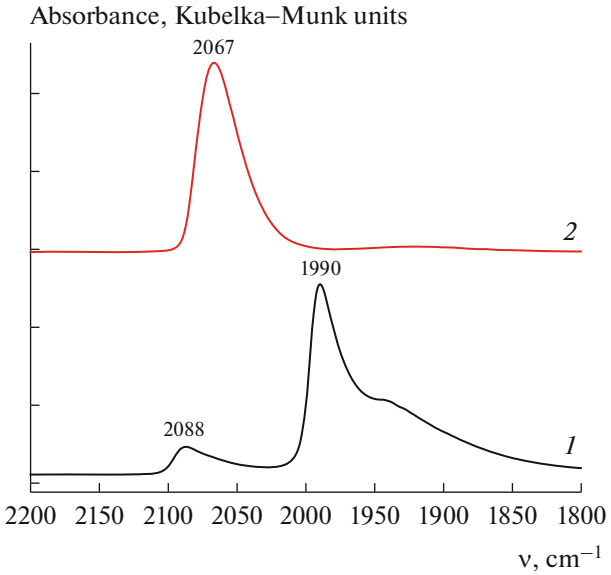

Fig. 2. DRIFTS spectra of adsorbed CO for the catalysts: (*1*) Pd/Al_2O_3 reference sample and (*2*) freshly reduced $PdIn/Al_2O_3$.

indicates the presence of well-crystallized supported palladium nanoparticles.

The spectrum of the reduced $PdIn/Al_2O_3$ catalyst contains a single peak with a maximum at 2067 cm^{-1}, which corresponds to the linear adsorption of CO on palladium atoms (spectrum *2*, Fig. 2). The shift of the absorption band toward lower wavenumbers is probably caused by a change in the electronic state of Pd atoms as a result of the formation of Pd–In covalent bonds [36, 37]. In addition, the bathochromic shift of the CO absorption band can be partially associated with a decrease in the degree of lateral interaction between the neighboring CO molecules due to the geometrical separation of Pd atoms by indium.

The absence of absorption bands in the region below 2000 cm^{-1} confirms the formation of the Pd_1In_1 intermetallic compound with a surface structure in which palladium atoms are separated from one another by indium atoms. This structure ensures the formation of isolated active Pd_1 sites on the catalyst surface and explains the absence of multi-point adsorption of CO, which requires the presence of several neighboring palladium atoms ("ensembles").

X-Ray Photoelectron Spectroscopy

Figure 3 shows the Pd3*d* and In3*d* spectra for the monometallic Pd/Al_2O_3 and In/Al_2O_3 and bimetallic $PdIn/Al_2O_3$ catalysts. The In/Pd atomic ratio calculated from the XPS data is 1.01, which corresponds to the stoichiometric composition of the Pd_1In_1 intremetallide and agrees with the XRD data.

Note that for Pd/Al_2O_3, the binding energy of the Pd3$d_{5/2}$ peak (BE = 334.9 eV) and its asymmetry are typical for palladium in the metallic state (Pd^0). For In/Al_2O_3, the binding energy of the In3$d_{5/2}$ peak is ~445.3 eV, which is typical of indium in the In^{3+} state (in In_2O_3). The shoulder on the side with lower binding energies (BE = 443.9 eV) can be attributed to indium in the metallic state. For Pd–In/Al_2O_3, the Pd3*d* peaks shifted toward higher binding energies, and the In3*d* peaks shifted toward lower binding energies relative to those of the monometallic samples. This suggests that the electronic properties of the active component changed. In [38, 39], where the PdIn bulk samples were studied, these shifts were explained in terms of the relatively simple model of charge transfer in the $Pd^{\delta+}$–$In^{\delta-}$ system. A decrease in the number of In–In bonds and, accordingly, an increase in the number of Pd–In bonds leads to a relative increase in electron density on indium atoms and thus to a shift of the In3*d* line toward lower binding energies. The positive shift of the Pd3*d* line is also expected because the palladium atoms in the PdIn intermetallics have a higher positive charge compared to metallic palladium in the Pd/Al_2O_3. Similar changes in the positions of the Pd3*d* and Ga3*d* lines were previously observed in the study of PdGa systems [40] and some other palladium-based intermetallics [41].

Note that, in addition to the shift of the Pd3*d* line, the peak asymmetry changes for the intermetallic PdIn catalyst: the peak becomes more symmetrical compared to the monometallic sample. The characteristic change in the shape of the photoelectron peaks is associated with the following effect. For metals in the solid state there is a distribution of unoccupied one-electron levels above the Fermi level, which can participate in the many electron shake-up effects accompanying the core electron emission [40, 42, 43]. In this case, a "tail" of inelastic losses is observed on the side with higher binding energies (i.e., lower photoelectron kinetic energies) in the core level spectrum. The lower the electron density of the states near the Fermi level, the lower the degree of asymmetry. Thus, the more symmetric peak shape in the case of the intermetallic PdIn sample indicates a decrease in the density of states near the Fermi level in the region of the top of the valence band compared to the same characteristic of the monometallic sample. This change in the electronic state of palladium atoms is in good agreement with published data. For example, a study of the formation of the Pd–In alloy as a result of In deposition on the surface of a Pd(111) single crystal [43] showed that the Pd3$d_{5/2}$ peak of the PdIn intermetallic compound shifted (by 0.65–0.9 eV) toward

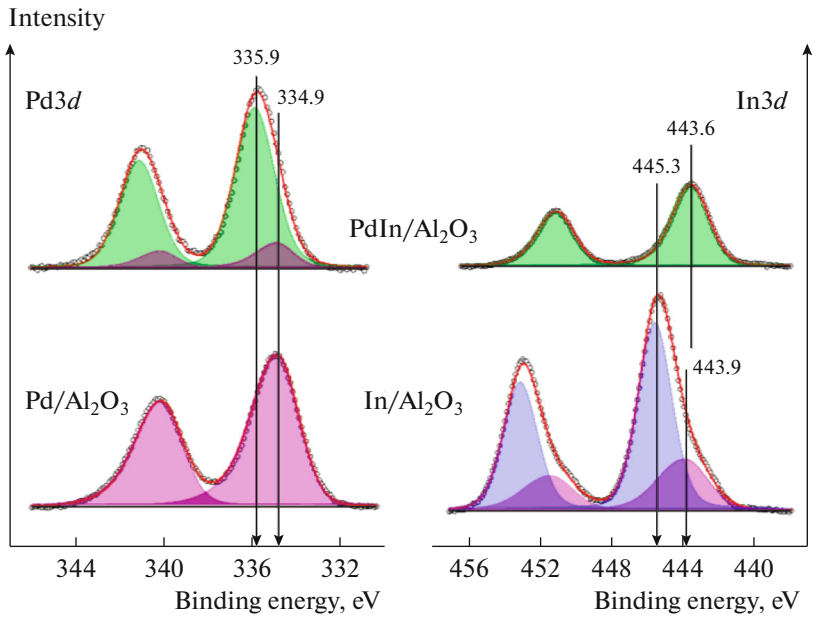

Fig. 3. Pd3*d* and In3*d* XPS spectra of the Pd/Al_2O_3 and In/Al_2O_3 monometallic samples and $PdIn/Al_2O_3$ bimetallic catalyst.

higher binding energies compared with the signal of the monometallic sample, and the Pd3*d* line of the intermetallics became more symmetric [43].

A change in the density of the *d* states near the Fermi level has a significant effect on the catalytic adsorption characteristics. Thus, a decrease in the density of states of Pd4*d* near the Fermi level during the formation of the ordered PdIn intermetallics compared with the density of states of Pd leads to a decrease in the adsorption energy of small molecules such as CO, H_2, and C_2H_2 on the surface of bimetallic nanoparticles [38, 39] and shows itself as a corresponding change in the catalytic properties (see below).

Analysis of Catalytic Properties in Gas-Phase Hydrogenation

The temperature dependences of acetylene conversion are presented in Fig. 4. The $PdIn/Al_2O_3$ sample is markedly less active than the monometallic reference sample: 100% conversion of acetylene on the PdIn catalyst requires a temperature of ~150°C, whereas on the Pd sample, complete conversion of C_2H_2 is achieved already at 115°C. The result is in good agreement with the published data. It was shown that on PdGa catalysts, acetylene completely transformed at temperatures higher than 200°C (Table 1) [44, 45].

An analysis of the temperature dependences using Arrhenius plots allows us to calculate the apparent activation energy of the process (Fig. 5). For the PdIn catalyst, E_a (45.9 kJ/mol) is significantly lower than for the palladium sample (71.8 kJ/mol). A similar effect was found in studies of acetylene hydrogenation on bimetallic catalysts [36, 46]. For $PdIn/Al_2O_3$, E_a decreases by 8 kJ/mol [36]; for PdAg, the calculated value of E_a is 12 kJ/mol lower than for the monometallic Pd analog [46].

Despite its lower activity, the $PdIn/Al_2O_3$ catalyst exhibits extremely high selectivity (Fig. 6). The selectivity remains almost constant (~94%) over a wide

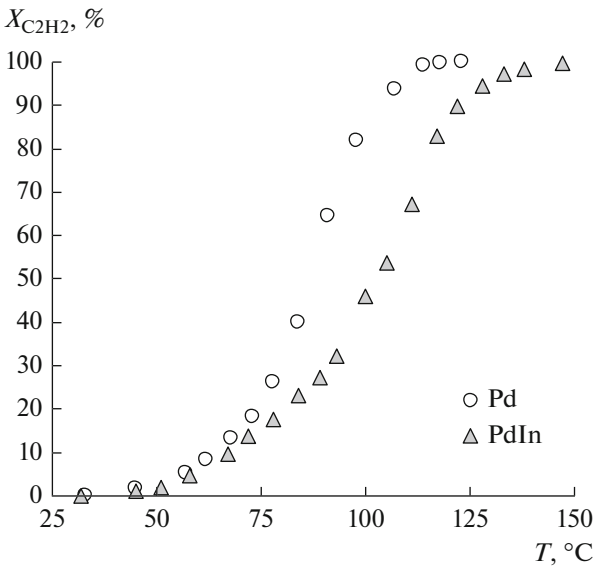

Fig. 4. Temperature dependence of acetylene conversion for the Pd/Al_2O_3 and $PdIn/Al_2O_3$ catalysts.

Table 1. Comparison of the catalytic characteristics of the Pd/Al_2O_3 and $PdIn/Al_2O_3$ samples obtained in this study with published data

Catalyst	$T_{100\%}$, °C*	$S_{90\%}$, %**	$C_2H_2 : C_2H_4 : H_2$	Ref.
Pd/Al_2O_3	114	57	1 : 90 : 5	This study
$PdIn/Al_2O_3$	147	93	1 : 90 : 5	This study
$GaPd/Al_2O_3$	>200	85	1 : 100 : 10	[44]
$GaPd_2/Al_2O_3$	>200	70–84	1 : 100 : 10	[44]
Pd_2Ga/CNT	>200	58	1 : 100 : 10	[45]
$Pd–Zn/Al_2O_3$	80	65	1 : 78 : 2	[51]
$Pd–Ag/Al_2O_3$	30–50	65***	1 : 36 : 10	[52]

* The temperature at which 100% conversion of C_2H_2 is reached.
** The selectivity of ethylene formation at 90% conversion of C_2H_2.
*** The selectivity of ethylene formation at 95% conversion of acetylene.

range of C_2H_2 conversions and slightly decreases to 86% only when complete conversion of acetylene is achieved. At the same time, for the monometallic sample, the selectivity gradually decreases over the whole range of acetylene conversions, changing most abruptly at conversions above ~40%. At 100% conversion of acetylene, the selectivity of the Pd catalyst decreases to ~35%.

The decreased selectivity observed at increased acetylene conversion is explained by two factors. Firstly, the increased acetylene conversion leads to increased ethylene concentration in the reaction medium and hence to increased hydrogenation rate (kinetic factor). Secondly, with a decrease in the concentration of acetylene, the amount of adsorbed C_2H_2 decreases, which blocks the surface of the catalyst due to the higher heat of adsorption and thus prevents the hydrogenation of ethylene (thermodynamic factor). After complete conversion of acetylene and its disappearance from the reaction medium the catalyst surface becomes fully accessible for adsorption of ethylene and its hydrogenation rate increases with a subsequent sharp decrease in selectivity.

A comparison of our results with the literature data (Table 1) allows us to conclude that the synthesized $PdIn/Al_2O_3$ intermetallic catalyst has extremely high selectivity (~94%) at 90% conversion of acetylene, while the selectivity of the best PdGa intermetallic systems does not exceed 85%.

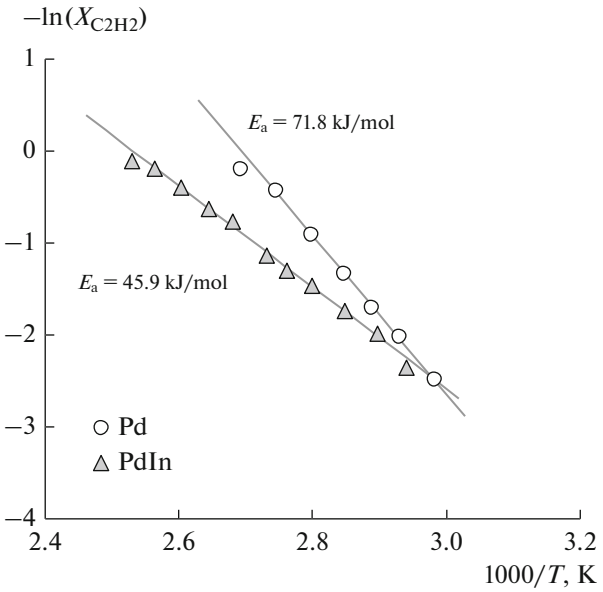

Fig. 5. Apparent activation energy of acetylene hydrogenation on the Pd/Al_2O_3 and $PdIn/Al_2O_3$ catalysts.

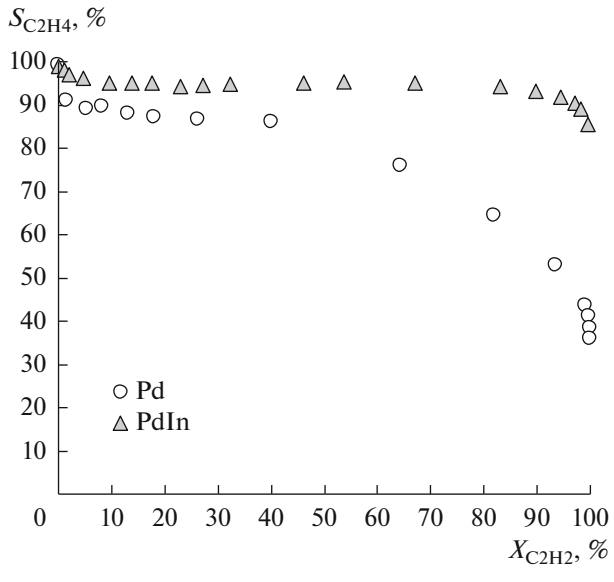

Fig. 6. Dependence of the selectivity of ethylene formation on acetylene conversion for the Pd/Al_2O_3 and $PdIn/Al_2O_3$ catalysts.

The observed changes in the catalytic characteristics agree well with the data of the physicochemical analysis and can be explained in terms of the model proposed in [47]. According to this model, the decreased heat of ethylene adsorption on the catalyst surface leads to increased selectivity in acetylene hydrogenation, facilitating the desorption of the resulting ethylene and hindering its further hydrogenation. On the other hand, a decrease in ethylene adsorption is usually accompanied by a decrease in acetylene adsorption, decreasing the rate of the whole process.

Interpreting our results within the framework of this model, we can conclude that the lower catalytic activity of the PdIn sample is caused by two factors: (1) a change in the structure of the active site (geometrical factor) and (2) a change in the electronic state of Pd (electronic factor). According to the FTIR-CO data, the active sites in the PdIn catalyst are Pd atoms isolated from one another by In atoms. As is known, a transformation of multiatomic active sites into monoatomic ones generally leads to a decrease in the adsorption energy of reagent molecules. For example, it was shown that the adsorption energy of ethylene on the Pt(111) and Pt_2Sn_3(110) faces decreased from −1.64 to −0.73 eV because of the formation of isolated Pt_1 sites on the Pt_2Sn_3(110) surface and the ensuing transformation of the adsorbed molecule from di-σ-bonded to π-bonded form [48]. A decrease in the binding energy of the ethylene molecule with the catalyst surface facilitates its desorption and lowers the probability of further hydrogenation [47, 49]. This assumption is confirmed by the theoretical calculations and experimental data for the PdIn(110) and Pd3In(111) faces, from which it follows that the presence of isolated Pd atoms is a key requirement for ensuring high ethylene selectivity [50].

In addition to the geometrical factor (modification of the structure of the active site), a significant role is also played by the electronic factor (modification of the electronic state of Pd as a result of the formation of the intermetallics). Thus, according to the XPS data, the formation of the Pd_1In_1 intermetallics affects the electronic state of Pd atoms and also significantly changes the structure of the valence band, decreasing the density of the *d* states near the Fermi level. As a result, the adsorption energy of both the initial acetylene and the intermediate hydrogenation product also decreases, lowering the activity, but increasing the process selectivity.

CONCLUSIONS

Thus, it can be concluded that the catalysts based on bimetallic PdIn nanoparticles have extremely high selectivity in the gas-phase hydrogenation of acetylene in the presence of ethylene and can thus be considered promising catalysts for selective catalytic removal of C_2H_2 impurities and homologs from pyrolysis ethane-ethylene fractions for subsequent polymerization. A comprehensive physicochemical study of the structure of the $PdIn/Al_2O_3$ catalyst by XRD, XPS, and IR spectroscopy of adsorbed CO indicates that the high selectivity is due to the formation of Pd_1In_1 intermetallic nanoparticles. As a result, highly homogeneous Pd_1 sites are formed on the surface of bimetallic nanoparticles, in which Pd atoms are isolated from one another by In atoms (geometrical factor). In addition, the formation of Pd–In bonds affects the electronic state of Pd atoms (electronic factor). Both factors lead to a change in the adsorption and catalytic characteristics, resulting in a sharp increase in the selectivity of the $PdIn/Al_2O_3$ catalyst in acetylene hydrogenation.

ACKNOWLEDGMENTS

We are grateful to M.N. Vargaftik and I.A. Yakushev for providing us with the sample of the bimetallic complex used for catalyst preparation.

FUNDING

The XRD, XPS, and IR spectroscopy studies of the structure and morphology of the catalysts and their catalytic characteristics in gas-phase hydrogenation of acetylene were financially supported by the Russian Scientific Foundation (grant no. 19-13-00285). The procedure for the synthesis of the bimetallic $PdIn/Al_2O_3$ catalyst was developed with financial support of the Russian Scientific Foundation (grant no. 16-13-10530).

REFERENCES

1. Furukawa, S. and Komatsu, T., *ACS Catal.*, 2017, vol. 7, p. 735.
2. Marakatti, V. S. and Peter, S. C., Prog. Solid State Chem., 2018, vol. 52, p. 1.
3. Armbrüster, M., Schlögl, R., and Grin, Yu., Sci. Technol. Adv. Mater., 2014, vol. 15, p. 034803.
4. Dasgupta, A. and Rioux, R.M., *Catal. Today*, 2019, vol. 330, p. 2.
5. Arkatova, L.A., *Khim. Interesah Ustoich. Razvit.*, 2001, vol. 19, p. 7.
6. Armbrüster, M., Behrens, M., Cinquini, F., Föttinger, K., Grin, Yu., Haghofer, A., Klötzer, B., Knop-Gericke, A., Lorenz, H., Ota, A., Penner, S., Prinz, J., Rameshan, C., Révay, Z., and Rosenthal, D., et al., *ChemCatChem.*, 2012, vol. 4, p. 1048.
7. Armbrüster, M., Kovnir, K., Behrens, M., Teschner, D., Grin, Yu., and Schlögl, R., *J. Am. Chem. Soc.*, 2010, vol. 132, p. 14745.

8. Kovnir, K., Armbrüster, M., Teschner, D., Venkov, T.V., Jentoft, F.C., Knop-Gericke, A., Grin, Yu., and Schlögl, R., *Sci. Tech. Adv. Mater.*, 2007, vol. 8, p. 420.
9. Osswald, J., Giedigkeit, R., Jentoft, R.E., Armbrüster, M., Girgsdies, F., Kovnir, K., Ressler, T., Grin, Yu., and Schlögl, R., *J. Catal.*, 2008, vol. 258, p. 210.
10. Osswald, J., Kovnir, K., Armbrüster, M., Giedigkeit, R., Jentoft, R.E., Wild, U., Grin, Yu., and Schlögl, R., *J. Catal.* 2008, vol. 258, p. 219.
11. Wowsnick, G., Teschner, D., Kasatkin, I., Girgsdies, F., Armbrüster, M., Zhang, A., Grin, Yu., Schlögl, R., and Behrens, M., *J. Catal.*, 2014, vol. 309, p. 209.
12. Wowsnick, G., Teschner, D., Armbrüster, M., Kasatkin, I., Girgsdies, F., Grin, Yu., Schlögl, R., and Behrens, M., *J. Catal.*, 2014, vol. 309, p. 221.
13. Kovnir, K., Osswald, J., Armbruster, M., Giedigkeit, R., Ressler, T., Grin, Yu., and Schlögl, R., *Stud. Surf. Sci. Catal.*, 2006, vol. 162, p. 481.
14. Glyzdova, D.V., Smirnova, N.S., Leont'eva, N.N., Gerasimov, E.Yu., Prosvirin, I.P., Vershinin, V.I., Shlyapin, D.A., and Tsyrul'nikov, P.G., *Kinet. Catal.* 2017, vol. 58, p. 140.
15. Afonasenko, T.N., Smirnova, N.S., Temerev, V.L., Leont'eva, N.N., Gulyaeva, T.I., and Tsyrul'nikov, P.G., *Kinet. Catal.* 2016, vol. 57, p. 490.
16. Smirnova, N.S., Shlyapin, D.A., Mironenko, O.O., Anoshkina, E.A., Temerev, V.L., Shitova, N.B., Kochubey, D.I., and Tsyrul'nikov, P.G., *J. Mol. Catal. A: Chem.*, 2012, vol. 358, p. 152.
17. Smirnova, N.S., Shlyapin, D.A., Shitova, N.B., Kochubey, D.I., and Tsyrul'nikov, P.G., *J. Mol. Catal. A: Chem.*, 2015, vol. 403, p. 10.
18. Smirnova, N.S., Mironenko, O.O., Shlyapin, D.A., Tsyrul'nikov, P.G., and Kochubei, D.I., *Bull. Russ. Acad. Sci.: Phys.*, 2013, vol. 77, p. 1151
19. Smirnova, N.S., Shlyapin, D.A., Leont'eva, N.N., Trenikhin, M.V., Shitova, N.B., Tsyrul'nikov, P.G., and Kochubei, D.I., *Bull. Russ. Acad. Sci.: Phys.*, 2015, vol. 79, p. 1186.
20. Furukawa, S., Takahashi, K., and Komatsu, T., *Chem. Sci.*, 2016, vol. 7, p. 4476.
21. Krajčí, M. and Hafner, J., *ChemCatChem.*, 2016, vol. 8, p. 34.
22. Furukawa, S., Endo, M., and Komatsu, T., *ACS Catal.* 2014, vol. 4, p. 3533.
23. Okamoto, H., *ASM Int.*, 2000, vol. 828, p. 2000.
24. Wu, Z., Wegener, E.C., Tseng, H.-T., Gallagher, J.R., Harris, J.W., Diaz, R.A., Ren, Ya., Ribeiro, F.H., and Miller, J.T., *Catal. Sci. Technol.*, 2016, vol. 6, p. 6965.
25. Mashkovsky, I.S., Markov, P.V., Bragina, G.O., Baeva, G.N., Rassolov, A.V., Yakushev, I.A., Vargaftik, M.N., and Stakheev, A.Yu., *Nanomaterials*, 2018, vol. 8, p. 769.
26. Burueva, D.B., Kovtunov, K.V., Bukhtiyarov, A.V., Barskiy, D.A., Prosvirin, I.P., Mashkovsky, I.S., Baeva, G.N., Bukhtiyarov, V.I., Stakheev, A.Yu., and Koptyug, I.V., *Chem. Eur. J.*, 2018, vol. 24, p. 2547.
27. Stakheev, A.Yu., Smirnova, N.S., Krivoruchenko, D.S., Baeva, G.N., Mashkovsky, I.S., Yakushev, I.A., and Vargaftik, M.N., *Mendeleev Commun.* 2017, vol. 27, p. 515.
28. Bard, A.J., Parsons, R., and Jordan, J., *Standard Potentials in Aqueous Solution*, Boca Raton: CRC Press, 1985, p. 848.
29. Mashkovsky, I.S., Smirnova, N.S., Markov, P.V., Baeva, G.N., Bragina, G.O., Bukhtiyarov, A.V., Prosvirin, I.P., and Stakheev, A.Yu., *Mendeleev Commun.* 2018, vol. 28, p. 603.
30. Stakheev, A.Yu., Highly organized nanostructured heterogeneous catalysts based on bimetallic and intermetallic nanoparticles for reactions of fine organic synthesis, *Report on the RSF project 16-13-10530 in 2018.* http://rscf.ru/prjcard/?rid=16-13-10530
31. Langford, J.I. and Wilson, A.J.C., *J. Appl. Crystallogr.*, 1978, vol. 11, p. 102.
32. Moulder, J., Stickle, W., Sobol, P., and Bomben, K., *Handbook of X-ray Photoelectron Spectroscopy*, Eden Priarie: Perkin-Elmer, 1992.
33. Scofield, J.H., *J. Electron Spectrosc. Relat. Phenom.*, 1976, vol. 8, p. 129.
34. Lear, T., Marshall, R., Lopez-Sanchez, J.A., Jackson, S.D., Klapotke, T.M., Baumer, M., Rupprechter, G., Freund, H.-J., and Lennon, D., *J. Chem. Phys.*, 2005, vol. 123, p. 174706.
35. Hadjiivanov, K.I. and Vayssilov, G.N., *Adv. Catal.*, 2002, vol. 47, p. 307.
36. Cao, Y., Sui, Z., Zhu, Y., Zhou, X., and Chen, D., *ACS Catal.*, 2017, vol.7, p. 7835.
37. Wencka, M., Hahne, M., Kocjan, A., Vrtnik, S., Kozelj, P., Korze, D., Jaglicic, Z., Soric, M., Popcevic, P., Ivkov, J., Smontara, A., Gille, P., Jurga, S., Tomes, P., and Paschen, S., et al., *Intermetallics*, 2014, vol.55, p. 56.
38. Rameshan, C., Lorenz, H., Mayr, L., Penner, S., Zemlyanov, D., Arrigo, R., Haevecker, M., Blume, R., Knop-Gericke, A., Schlögl, R., and Klötzer, B., *J. Catal.*, 2012, vol. 295, p. 186.
39. Neumann, M., Teschner, D., Knop-Gericke, A., Reschetilowski, W., and Armbrüster, M., *J. Catal.*, 2016, vol. 340, p. 49.
40. Rameshan, C., Stadlmayr, W., Penner, S., Lorenz, H., Mayr, L., Hävecker, M., Blume, R., Rocha, T., Teschner, D., Knop-Gericke, A., Schlögl, R., Zemlyanov, D., Memmel, N., and Klötzer, B., *J. Catal.*, 2012, vol. 290, p. 126.
41. Hillebrecht, F.U., Fuggle, J.C., Bennett, P.A., and Zołnierek, Z., *Phys. Rev. B*, 1983, vol. 27, p. 2179.
42. *Practical surface analysis by Auger and X-ray photoelectron spectroscopy*, Briggs, D. and Seah, M.P., Eds., Chichester: Wiley, 1983.
43. McGuirk, G.M., Ledieu, J., Gaudry, É., de Weerd, M.-C., and Fournée, V., *J. Chem. Phys.*, 2014, vol. 141, p. 084702.

44. Armbrüster, M., Wowsnick, G., Friedrich, M., Heggen, M., and Cardoso-Gil, R., *J. Am. Chem. Soc.*, 2011, vol. 133, p. 9112.

45. Shao, L.D., Zhang, W., Armbrüster, M., Teschner, D., Girgsdies, F., Zhang, B.S., Timpe, O., Friedrich, M., Schlögl, R., and Su, D.S., *Angew. Chem.*, 2011, vol. 50, p. 10231.

46. Pei, G.X., Liu, X.Y., Wang, A., Lee, A.F., Isaacs, M.A., Li, L., Pan, X., Yang, X., Wang, X., Tai, Z., Wilson, K., and Zhang, T., *ACS Catal.*, 2015, vol. 5, p. 3717.

47. Studt, F., Abild-Pedersen, F., Bligaard, T., Sørensen, R.Z., Christensen, C.H., and Nørskov, J.K., *Science*, 2008, vol. 320, p. 1320.

48. Meyer, R.J., Zhang, Q., Kryczka, A, Gomez, C., and Todorovic, R., *ACS Catal.*, 2018, vol. 8, p. 566.

49. Osswald, J., Active-site isolation for the selective hydrogenation of acetylene: the Pd-Ga and Pd–Sn intermetallic compounds, PhD Thesis, Berlin: Technical Univeristy Berlin, 2006, p. 163.

50. Feng, Q., Zhao, S., Wang, Y., Dong, J., Chen, W., He, D., Wang, D., Yang, J., Zhu, Y., Zhu, H., Gu, L., Li, Z., Liu, Y., Yu, Rong., Li, J., and Li, Y., *J. Am. Chem. Soc.*, 2017, vol. 139, p. 7294.

51. Mashkovskii, I.S., Tkachenko, O.P., Baeva, G.N., and Stakheev, A.Yu., *Kinet. Catal.* 2009, vol. 50, p. 768.

52. Lamberov, A.A., Egorova, S.R., Il'yasov, I.R., Gil'manov, Kh.Kh., Trifonov, S.V., Shatilov, V.M., and Ziyatdinov, A.Sh., *Kinet. Catal.* 2007, vol. 48, p. 136.

Translated by L. Smolina